

XMM-Newton observations of the nearby brown dwarf LP 944-20

Eduardo L. Martín

Institute for Astronomy, 2680 Woodlawn Drive, Honolulu Hawai'i, 96822, USA

ege@teide.ifa.hawaii.edu

and

Hervé Bouy

E.S.O, Karl Schwarzschildstraße 2, D-85748 Garching, Germany

hbouy@eso.org

ABSTRACT

The nearby ($d = 5.0$ pc) brown dwarf LP 944-20 was observed with the *XMM-Newton* satellite on 07 January 2001. The target was detected with the Optical Monitor ($V = 16.736 \pm 0.081$), but it was not detected during the ≈ 48 ks observation with the X-ray telescopes. We determine a 3σ upper limit for the X-ray emission from this object of $L_X < 3.1 \times 10^{23} \text{ ergs} \cdot \text{s}^{-1}$, equivalent to a luminosity ratio upper limit of $\log(L_X/L_{bol}) \leq -6.28$. This measurement improves by a factor of 3 the previous *Chandra* limit on the quiescent X-ray flux. This is the most sensitive limit ever obtained on the quiescent X-ray emission of a brown dwarf. Combining the *XMM-Newton* data with previous *ROSAT* and *Chandra* data, we derive flare duty cycles as a function of their luminosities. We find that very strong flares [$\text{Log}(L_X/L_{bol}) > -2.5$] are very rare (less than 0.7% of the time). Flares like the one detected by *Chandra* [$\text{Log}(L_X/L_{bol}) = -4.1$] have a duty cycle of about 6%, which is lower than the radio flare duty cycle ($\sim 13\%$). When compared with other M dwarfs, LP 944-20 appears to be rather inactive in X-rays despite of its relative youth, fast rotation and its moderately strong activity at radio wavelengths.

Subject headings: individual: LP 944-20 — stars : brown dwarfs, low-mass — stars : X-ray emission

1. Introduction

LP 944–20 (=BRI 0337-3535) is an isolated nearby brown dwarf (Mass $<0.075 M_{\odot}$) first identified by Luyten & Kowal (1975). Spectroscopic observations reported by Tinney (1998) give a spectral type of dM9, an age of about 500 Myr and a mass of about $0.065 M_{\odot}$ using the lithium test proposed by Magazzù, Martín, & Rebolo (1993). Because of its substellar mass and its proximity to the Sun, this object is a benchmark in the study of very low-mass objects. LP 944–20 was observed in the X-Ray regime for the first time with the *ROSAT* satellite by Neuhäuser et al. (1999), but was not detected. It has been detected with the *Chandra* satellite (Rutledge et al. 2000) in december 1999 during an X-ray flare of duration $1 \sim 2$ hours. Outside the flare, LP 944–20 was not detected with a 3σ upper limit on the emission at $L_X < 1.0 \times 10^{24} \text{ ergs} \cdot \text{s}^{-1}$. Both quiescent and flaring radio emission have been observed with the VLA (Berger et al. 2001).

X-ray emission is widespread among fully-convective M dwarfs (spectral type M3 and later), and it is frequently variable (Fleming et al. 1993; Marino, Micela & Peres 2000; Feigelson et al. 2002). X-ray observations of ultracool dwarfs (spectral type M7 and later) are still very scarce. Strong variability has been observed in a few objects (Rutledge et al. 2000; Fleming et al. 2000; Schmitt & Liefke 2002). It is thought that the X-ray photons are emitted from a hot corona. The properties of coronae (permanent or transient) in ultracool dwarfs are not well understood.

LP 944–20 was targeted for observations with *XMM-Newton* for two reasons mainly, first to try to catch it during a flare, which would have allowed to obtain spectroscopy if a flare had occurred, and second to search for quiescent X-ray emission. Unfortunately, we did not detect LP 944–20 at all. Nevertheless, we improve the value of the upper limit on the quiescent X-ray emission from LP 944–20, and we derive X-ray flare rates as a function of X-ray luminosity that may be useful for planning future observations of this brown dwarf.

2. Observations

XMM-Newton observed LP 944–20 on 2001 January 07-08, between 14:21:05 and 04:43:52 UTC for 51767 s. The pointing position was $R.A. = 03\text{h}39\text{min}34.60\text{sec}$ and $Dec = -35^{\circ}25''51.0'$ Epoch 2000, according to the Simbad database.¹

¹Simbad database, operated at CDS, Strasbourg, France

2.1. Optical Data and Source Identification

Besides its three X-ray telescopes, *XMM-Newton* also has a 30-cm optical-UV telescope, providing the possibility to observe simultaneously in the X-ray and optical-UV regimes. The Optical Monitor (*OM*) was used with the *V* filter for four exposures of 5000 s each in imaging mode. The OM detector has a format of 2048×2048 pixels, each $0.5'' \times 0.5''$. The field of view is therefore $17' \times 17'$.

We used the data given by the OM to confirm the presence of the source in the field of view. The coordinates we used to identify LP 944–20 are different from the pointing coordinates. We used the more recent coordinates given by the astrometry of Rutledge et al. (2000) after their observation of LP 944–20 with *Chandra* during a X-ray flare in 1999 December. These coordinates are: $R.A. = 03\text{h}39\text{min}35.16\text{sec} \pm 0.1''$ and $Dec = -35^\circ 25' 44.0'' \pm 0.1''$, epoch 1999.95.

We identified LP 944–20 in the field of view by plotting these coordinates on the four images given by the OM. The result is shown in Figure 1. We found a point-source at a distance of $0.4'' \pm 0.1''$ from the expected coordinates of LP 944–20. This offset is small in comparison with the $< 2''$ known systematic uncertainties in the *XMM-Newton* preprocessing analysis astrometry (*XMM-Newton* User’s Handbook 2000). Moreover a small offset was also expected because of the proper motion of LP 944–20 since it was observed by Rutledge et al. (2000) more than one year ago. The offset in the optical position is consistent with the known proper motion of LP 944–20. We were also able to identify the three other sources in the field of view simply by direct comparison with the image obtained by Rutledge et al. (2000). We therefore identify this optical source with the brown dwarf LP 944–20 on the basis of positional coincidence with the expected coordinates.

We also used the four exposures given by the OM to look for optical variability. The magnitudes of the source identified as LP 944–20 and of two other stars in the field of view were calculated using the *IRAF phot* task. This allowed us to plot the evolution of the magnitude during the whole observation. The result is shown in Figure 2. The behavior of LP 944–20’s magnitude is different than that of the two other stars. We notice that whereas the magnitudes of the two reference stars are roughly correlated, LP 944–20’s magnitudes are not. We measure a mean magnitude of $V = 16.736$ and a standard deviation of 0.081 for LP 944–20. For reference star 1 we measure a mean magnitude of $V = 16.681$ and a standard deviation of 0.028. For reference star 2 we measure a mean magnitude of $V = 16.770$ and a standard deviation of 0.067. We conclude that LP 944–20 may be variable in the OM data. The variability of LP 944–20, however, is only slightly higher than that of reference star 2. We cannot make a definitive claim that LP 944–20 is variable in our data because of the lack of enough reference stars in the field of view.

2.2. X-ray Data and Analysis

The European Photon Imaging Camera (*EPIC*) MOS1 & MOS2 were used. The total ontarget exposure time in each camera was 48724 s in prime full window mode with 2.5 s time resolution. The EPIC PN was used in prime full window mode with 73.4 ms time resolution and ontarget exposure 46618 s. Each EPIC instrument was used with the thin filter, which suppresses the optical contamination up to m_V of 18 (MOS) or m_V of 17 (PN). Both MOS & PN detectors have a circular field of view of 30' diameter. For more details on *XMM-Newton* and its instruments, we refer to *XMM-Newton User's Handbook* (2000).

The first step was to search for LP 944–20 in the field of view of each EPIC MOS & PN detector. We plotted the coordinates of LP 944–20 on each image obtained by each detector, but we did not detect any source. To be sure that we were using the most sensitive exposure, we used the image given by the pipeline which combines data from all EPIC's MOS & PN in the entire energy range (0.1 – 12.0 keV), as shown in Figure 3.

On these figures, the X-ray source closest to the expected position is offset by $\delta(R.A.) = 2.5'' \pm 0.1''$ and $\delta(Dec) = -28.37'' \pm 0.1''$. This offset is large in comparison with the $0.4'' \pm 0.1''$ offset observed with the optical data. So at this point we already knew that LP 944–20 was not detected.

We performed differential astrometry between the *XMM-Newton* and *Chandra* images. This allowed us to identify all the X-ray sources in our field of view in an area of $20'' \times 10''$ centered on the expected coordinates of LP 944–20. We were then able to conclude that LP 944–20 was not detected during the *XMM-Newton* observation.

Since the target was not detected, the first conclusion is that there was no significant X-ray flare during this 48 ks observation. Nevertheless, it is interesting to calculate the upper limit on the time average quiescent X-ray luminosity. We did the calculation of the upper limit of X-ray flux with each of the 3 images of the preprocessing products, corresponding to the 3 exposures obtained with the EPIC MOS1, MOS2 & PN detectors on the entire energy range (0.1 – 12.0 keV). To calculate a 3σ flux upper limit, we considered an area of twice the FWHM (= 2 pixels) around the expected position of LP 944–20. In this area we calculated the mean value of $counts \cdot pixel^{-1}$ and the corresponding standard deviation σ using the IRAF² `phot` task, which gives count rates corrected for background. The results are listed in Table 1. As the EPIC PN camera is the most sensitive detector, we therefore only consider its result to calculate the flux upper limit.

²IRAF is distributed by National Optical Astronomy Observatory, which is operated by the Association of Universities for Research in Astronomy, Inc., under contract with the National Science Foundation.

To convert this count rate to flux, we followed XMM–Newton User’s Handbook (2000) instructions, by using the PIMMS³ software. As LP 944–20 was not detected during the observation, we were not able to fit its spectrum in order to know its spectral type. We adopted the results of Rutledge et al. (2000) summarized in Table 2. The HI column density was calculated using the nH^3 software: $n_H = 1.31 \times 10^{20} \text{ cm}^{-2}$.

The results for the upper limit of flux and X-ray luminosity (3σ , assuming Gaussian statistics) are listed in Table 3. The uncertainties on these values are Poisson (counting statistics) plus $\sim 10\%$ spectral uncertainty, according to Rutledge et al. (2000). As their best fit on the spectrum was obtained with the Raymond–Smith thermal plasma model, we finally kept the corresponding 3σ flux as the upper limit on the time average quiescent X-ray luminosity for LP 944–20: $L_X < 3.1 \times 10^{23} \text{ ergs} \cdot \text{s}^{-1}$, equivalent to a luminosity ratio upper limit of $\log(L_X/L_{bol}) \leq -6.28$.

3. Discussion

The first observation of LP 944–20 in the X-ray regime by Neuhäuser et al. (1999) with the *ROSAT* satellite placed an upper limit of $\log(L_X/L_{bol}) \leq -4.17$ after a 220 ks *ROSAT*–*HRI* observation. The second X-ray observation (Rutledge et al. 2000) placed a better upper limit of $\log(L_X/L_{bol}) \leq -5.70$ after the 44 ks *Chandra*–*ACIS-S* observation before the flare. Our new value improves this upper limit of quiescent X-ray emission at $\log(L_X/L_{bol}) \leq -6.3$. The corresponding upper limit of X-ray luminosity ($L_X \leq 3.1 \times 10^{23} \text{ ergs} \cdot \text{s}^{-1}$) is thus improved by a factor 3. This value is close to the solar X-ray emission level during its maxima of activity.

In Figure 4 we display the dependence of X-ray activity versus spectral type for M dwarfs. The upper envelope of X-ray activity is remarkably independent of M subclass. There is no obvious connection between age and X-rays. The M dwarfs in the ChaI, ρ Oph and Taurus star-forming regions show X-ray emission comparable to much older field dwarfs (Neuhäuser et al. 1999; Mokler & Stelzer 2002). We conclude that there is no evidence for a decline in coronal emission with increasing age in fully convective M dwarfs.

We have estimated the rate of X-ray flare occurrence in LP 944–20 by adding 287.5 ks of *ROSAT* data analyzed by Neuhäuser et al. (1999), 43.8 ks of *Chandra* data analyzed by Rutledge et al. (2000) and 51.7 ks of *XMM–Newton* data (this paper). The duration of the

³ nH and *PIMMS* (Portable, Interactive, Multi-Mission Simulator) are distributed by the NASA’s HEARSAC

only flare so far observed was 2.76 ks Rutledge et al. (2000). Thus, we get an X-ray flare frequency of 0.72% for flares with luminosity $\text{Log}(L_X/L_{bol}) > -2.5$. Weaker flares could not have been detected by *ROSAT*. Thus, we derive the duty cycle of flares with luminosity comparable with the flare detected by *Chandra* [$\text{Log}(L_X/L_{bol}) = -4.1$] to be about 6%.

The published VLA radio data have a duration of 79.9 ks (Berger et al. 2001). Three flares were detected with a total duration of ~ 10.4 ks. Hence, we estimate a radio flare frequency of about 13%. It is not known to what X-ray luminosity the radio flares correspond, but we can set an upper limit using the *XMM-Newton* data. If we assume a flare duty cycle of 13%, the flare X-ray luminosity has to be $\text{Log}(L_X/L_{bol}) < -5.39$ to be consistent with our non detection.

LP 944–20 is a relatively inactive object. Tinney (1998) reported H_α weakly in emission. Berger et al. (2001) estimated a surface magnetic field strength of $B \sim 5\text{G}$ assuming synchrotron emission during the radio flares. For comparison, active dM stars have magnetic field strengths of a few kG, solar flares have $B \sim 100\text{G}$, and Jupiter has an average $B \sim 10\text{G}$ (Hide & Stannard 1976). Our low upper limit on the quiescent X-ray emission of LP 944–20 is consistent with a weak magnetic field. The detection of low-amplitude photometric variability in LP 944–20, and the low-level of X-ray emission in this object, suggests the presence of surface thermal inhomogeneities due to nonmagnetic clouds, as discussed by Tinney & Tolley (1999) for LP 944–20 and by Martín, Zapatero Osorio, & Lehto (2001) for the M9.5 dwarf BRI0021-0214. Recent theoretical works (Gelino et al. 2002; Mohanty et al. 2002) show that in ultracool dwarfs there should not be much interaction between the gas and the magnetic field because the Reynolds number is very low throughout the photosphere.

LP 944–20 appears to be an object with substellar mass, weak magnetic field, fast rotation and cloudy atmosphere. We speculate that the radio activity may be enhanced by the presence of a close planetary-mass companion (Io-type), which provides a continuous supply of ionized particles to the ionosphere of LP 944–20. Radial velocity variability has been detected by Guenther & Wuchterl (2003) which could be due to a planetary-mass close companion, but they did not have enough data to derive an orbital period.

This research has made use of the Simbad ³ database, operated at CDS, Strasbourg, France. Support for this project has been provided by NASA grant NAG5-9992. We thank our collaborators Gibor Basri, Lars Bildsten and Bob Rutledge, and an anonymous referee for helpful discussions.

REFERENCES

- Berger, E., Ball, S., Becker, K. M., Clarkes, M., et al. 2001, *Nature* 410, 338
- Feigelson, E. D., Broos, P., Gaffney, J. A., Garmier, G., Hillenbrand, L. A., Pravdo, S. H., Townsley, L., & Tsuboi, Y. 2002, *ApJ*574, 258
- Fleming, T. A., Giampapa, M. S., Schmitt, J. H. M. M., & Bookbinder, J. A. 1993, *ApJ*410, 387
- Fleming, T. A., Schmitt, J. H. M. M., & Giampapa, M. S. 1995, *ApJ*450, 401
- Fleming, T. A., Giampapa, M. S., Schmitt, J. H. M. M. 2000, *ApJ*533, 372
- Gelino, C. R., Marley, M. S., Holtzman, J. A., Ackerman, A. S., & Lodders, K. 2002, *astroph-005305*
- Giampapa, M. S., Rosner, R., Kashyaf, V., Fleming, T. A., Schmitt, J. H. M. M., & Bookbinder, J. A. 1996, *ApJ*463, 707
- Guenther, E. & G. Wuchterl 2003, in *IAU Symposium 211: Brown Dwarfs*, E. L. Martín (ed.), in press
- Hide, R. & Stannard, D. 1976, in *Jupiter*, T. Gehrels (ed.), The University of Arizona Press, Tucson
- Luyten, W. J., & Kowal, C. T. 1975, *Proper Motion Survey with the 48 inch Schmidt Telescope. XLIII. One Hundred and Six Faint Stars with Large Proper Motion* (University of Minnesota, Minneapolis).
- Magazzù, A., Martín, E. L., & Rebolo, R. 1993 *ApJ*, 404, L17
- Marino, A., Micela, G., & Peres, G. 2000, *A&A*353, 177
- Martín, E. L., Zapatero Osorio, M. R. & Lehto, H. 2001, *ApJ*, 557, 822

³<http://simbad.u-strasbg.fr/>

- Mohanty, S., Basri, G., Shu, F., Allard, F., & Chabrier, G. 2002, *ApJ*, 571, 469
- Mokler, F., & Stelzer, B. 2002, *A&A*, in press
- Neuhäuser, R., et al. 1999, *A&A*, 343, 883
- Rutledge, R. E., Basri, G., Martín, E. L, Bildsten, L., 2000, *ApJ*, 538L, 141
- Schmitt, J. H. M. M. & Liefke, C. 2002, *A&A*, 382, L9
- Tinney, C. G. 1996, *MNRAS*. 281, 644
- Tinney, C. G. 1998, *MNRAS*. 296, L42
- Tinney, C. G. & Tolley 1999, *MNRAS*. 304, 119
- XMM–Newton SOC Team, XMM–Newton User’s Handbook Issue 2, 03.31.2000

Table 1. Count rates

Instrument	Counts/pixel (average)	Standart deviation σ (counts/pixel)	3σ (counts/pixel/s)
EPIC PN	4.53	2.00	1.3×10^{-4}
EPIC MOS1	1.59	1.18	7.3×10^{-5}
EPIC MOS2	1.73	1.24	7.6×10^{-5}

Table 2. Spectral parameters of LP 944–20

Model	Associated Feature
Black Body	$k_B \times T = 0.17 \text{ keV}$
Power Law	$\alpha_{\text{photon}} = 2.6$
Thermal Plasma	$k_B \times T = 0.26 \text{ keV}$

References. — Rutledge et al. (2000)

Table 3. X-ray luminosity upper limit

Model	Flux ($10^{-17} \text{ erg.cm}^{-2}.\text{s}^{-1}$)	$\log L_X$ ($\text{ergs}.\text{s}^{-1}$)	$\log (\frac{L_X}{L_{bol}})$
Black Body	≤ 1.1	≤ 23.50	≤ -6.27
Power Law	≤ 1.3	≤ 23.59	≤ -6.19
Thermal Plasma	≤ 1.0	≤ 23.49	≤ -6.28

References. — Tinney (1996) for $L_{bol} \sim 6 \times 10^{29} \text{ ergs}.\text{s}^{-1}$

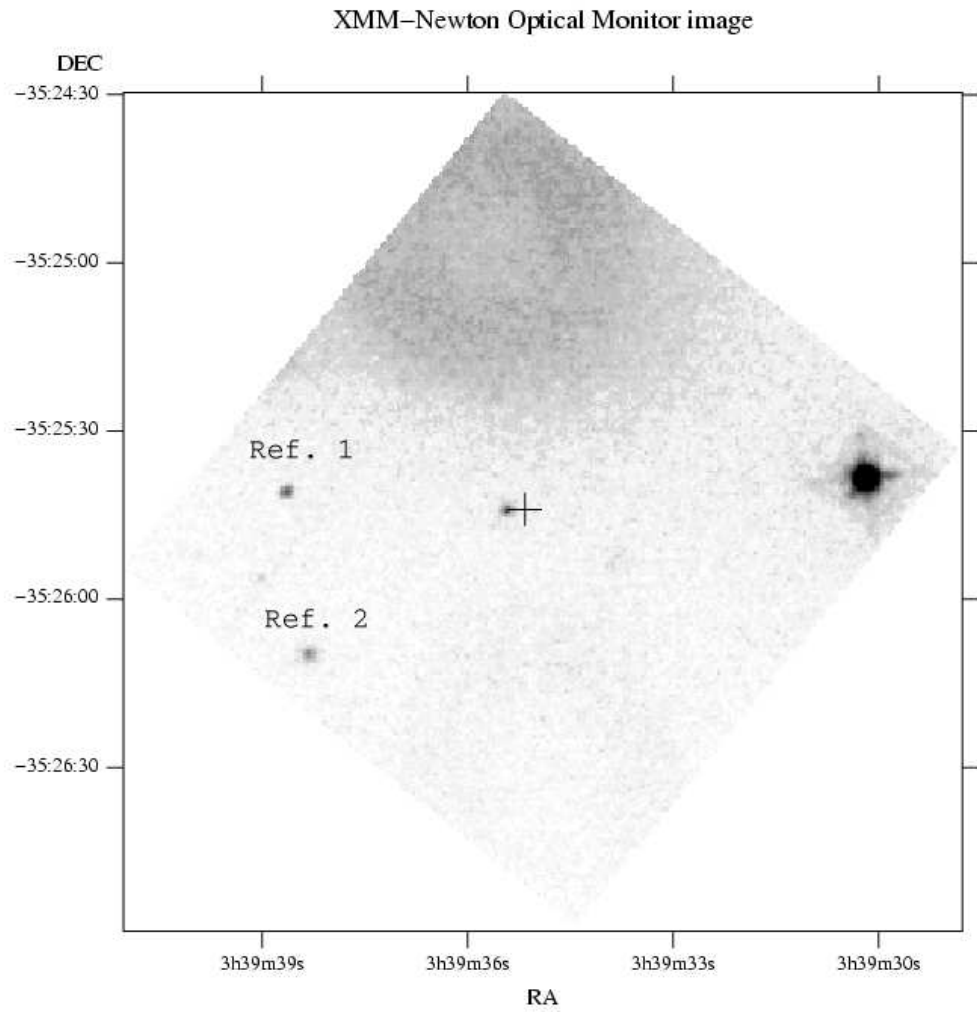


Fig. 1.— Identification of LP 944-20 in the field of view of the Optical Monitor Data. The plus indicate the expected coordinates of LP 944-20. The diffuse bright area on the top of the image is an artifact.

Magnitude in V vs. Time

XMM Optical Monitor

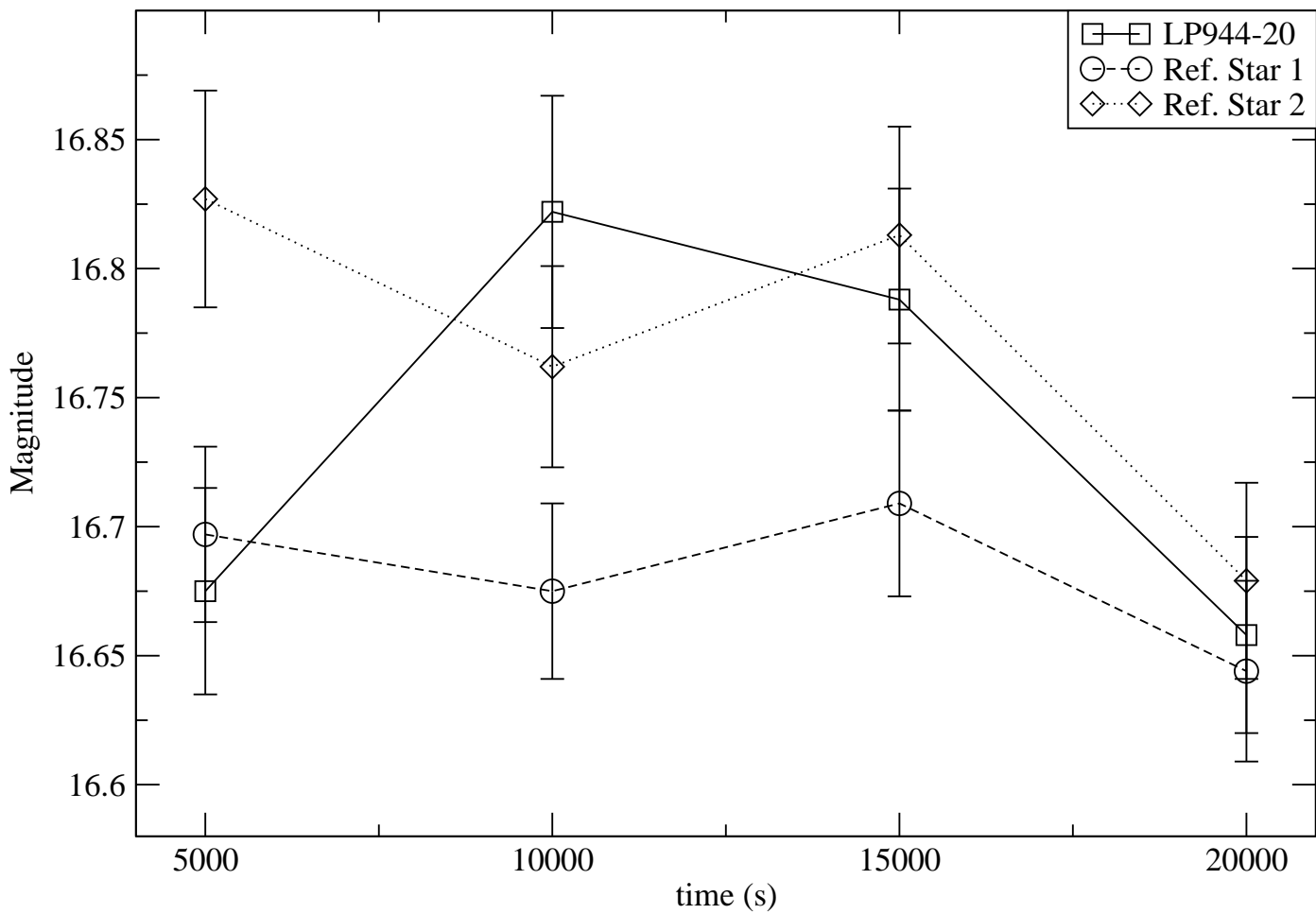


Fig. 2.— Optical magnitude of LP 944–20 and of 2 reference stars in the field of view of the Optical Monitor.

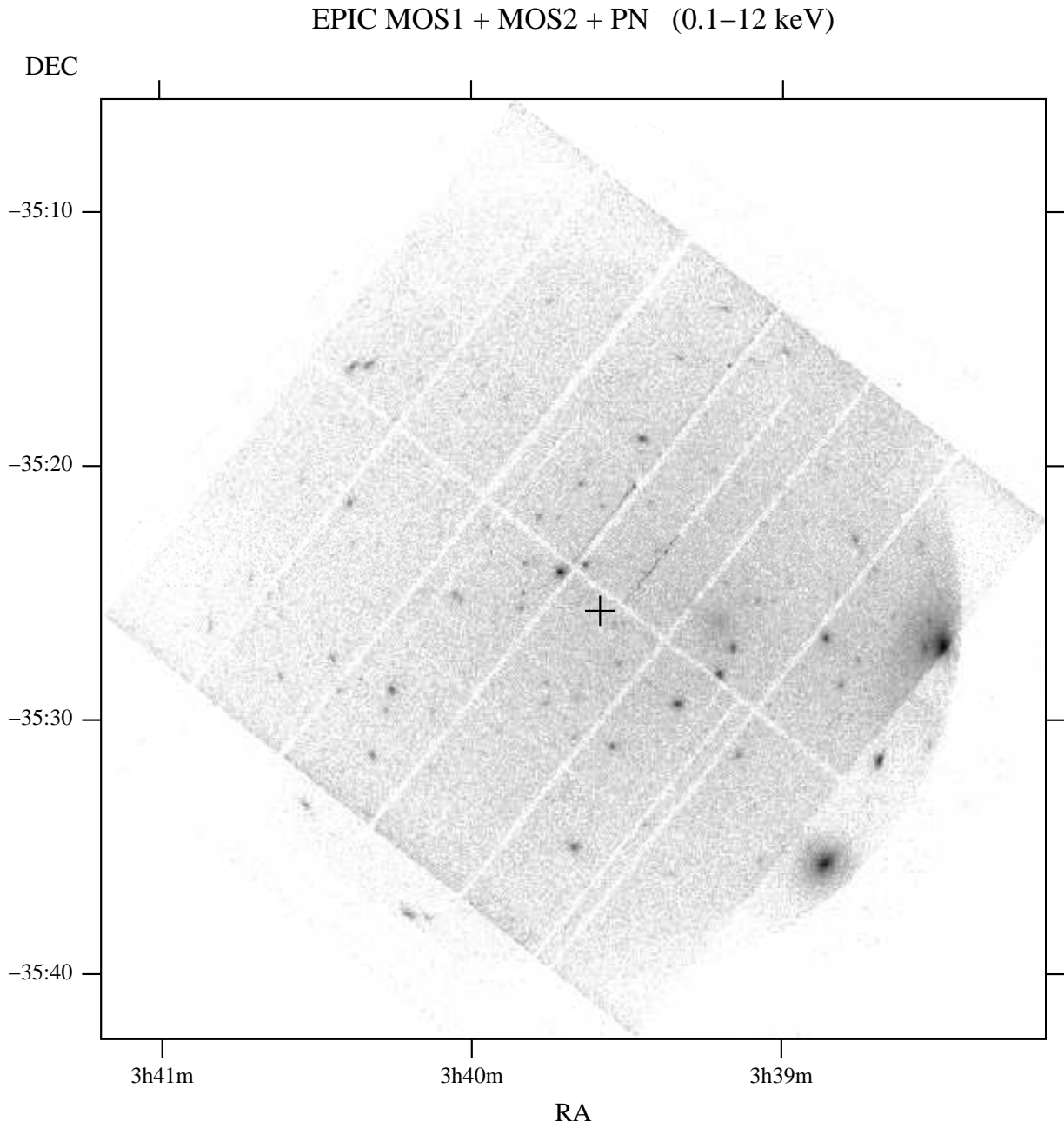


Fig. 3.— Combined image from all EPICs MOS & PN instruments in the energy range (0.1 – 12.0 keV). The figure shows the entire field of view. The square chips of the EPIC PN and the circular field of view of MOS1 & 2 appear on this figure. A plus indicate the expected position of LP 944–20.

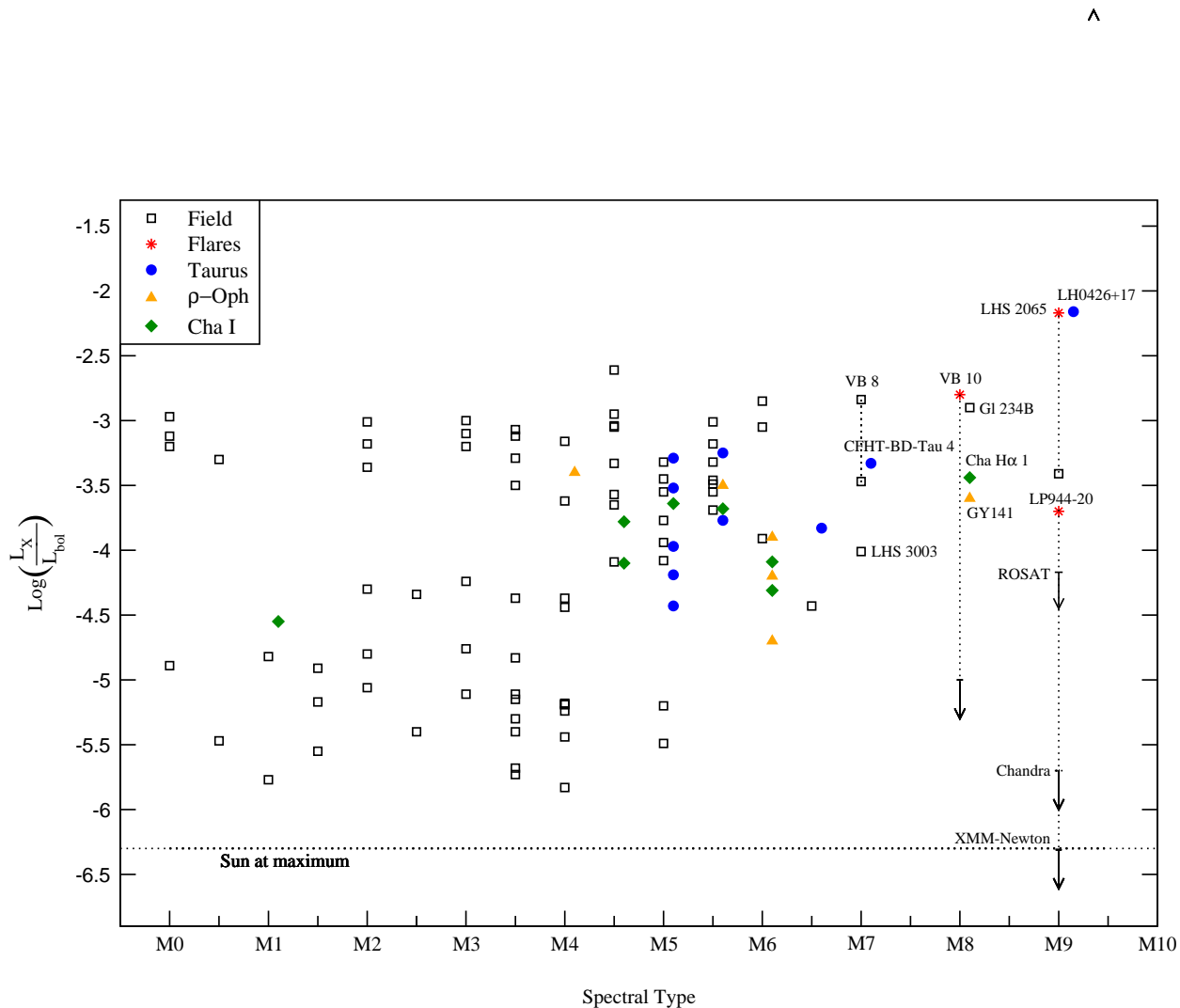


Fig. 4.— Distribution of X-ray luminosity of dM dwarfs as a function of spectral type. The squares represent values obtained for field dwarfs (Fleming et al. (1993); Fleming, Schmitt, & Giampapa (1995); Fleming et al. (2000); Giampapa et al. (1996); Rutledge et al. (2000)). The circles, diamonds and triangles denote young objects in star-forming regions. The stars represent the flaring objects at their maximum with the corresponding value or upper limit on the quiescent emission linked by a dotted line. To avoid confusion, the Taurus object’s spectral types have been shifted by 0.1 subclass.